Frontiers in Bioscience Landmark

Front. Biosci. (Landmark Ed) **2026**; 31(5): 50459
https://doi.org/10.31083/FBL50459

Original Research

Fabrication and Characterization of Silk-Fibroin, Polyvinyl Alcohol, and Natural Compounds-Derived Bioscaffold to Accelerate Wound Healing

Shubhra Sinha[1,†], Jekhan Andimadam Madana Saravanan[1,2,†], Azam Ali[2,3], Rajesh Katare[1,*]

[1]Department of Physiology, Heart Otago, School of Biomedical Sciences, University of Otago, 9016 Otago, New Zealand
[2]Centre of Bioengineering and Nanomedicine, Faculty of Dentistry, University of Otago, 9016 Otago, New Zealand
[3]Sir John Walsh Research Institute, Department of Oral Rehabilitation, Faculty of Dentistry, University of Otago, 9016 Otago, New Zealand
*Correspondence: rajesh.katare@otago.ac.nz (Rajesh Katare)
[†]These authors contributed equally.

Academic Editor: Francesca Diomede
Submitted: 28 January 2026 Revised: 13 April 2026 Accepted: 22 April 2026 Published: 25 May 2026

Abstract

Background: Impaired wound healing represents a significant clinical challenge. Persistent inflammation, excessive reactive oxygen species, and impaired angiogenesis are key mechanisms underlying nonhealing ulcers. We developed a multifunctional bioscaffold incorporating natural bioactive compounds as a mechanistic therapeutic strategy. **Methods**: Polyvinyl alcohol and silk fibroin formed the scaffold matrix, blended with Manuka honey, fenugreek seed extract, and Ghrelin for their antioxidant and proangiogenic properties. **Results**: Scanning electron microscopy revealed defect-free nanofibers with diameters below 200 nm. Fourier-transform infrared analysis confirmed successful incorporation of the bioactive components, indicating effective interactions within the polyvinyl alcohol (PVA)-silk fibroin (SF) matrix. Thermal analysis demonstrated improved thermal stability upon addition of the bioactive agents. The 3-(4,5-dimethylthiazol-2-yl)-2,5-diphenyltetrazolium bromide (MTT) assay confirmed the absence of toxicity. Scratch assays confirmed enhanced migration of human umbilical vein endothelial cells, supporting the scaffold's angiogenic potential. Additionally, the scaffold exhibited superior antioxidant activity and significantly improved cell proliferation. **Conclusions**: These findings demonstrate that the developed bioscaffold integrates antioxidant and proangiogenic properties, making it a promising candidate for various biomedical applications, particularly in wound dressings, drug delivery, tissue engineering, and biosensing.

Keywords: wound healing; nanofibers; Manuka honey; fenugreek seeds; ghrelin; angiogenesis; reactive oxygen species

1. Introduction

Skin injury is one of the most common clinical conditions requiring timely intervention to prevent further infection. Skin wounds represent a significant clinical and healthcare challenge, affecting an estimated 1–2% of individuals in developed countries over their lifetime [1]. As our population continues to age, along with the increasing prevalence of conditions such as diabetes and hypertension, it is important to address the expected rise in nonhealing wounds [2], especially since they are associated with increased reactive oxygen species (ROS), persistent infection [3], prolonged inflammation, impaired angiogenesis, and high tendency for secondary infection [4]. Current treatments, such as skin grafts and allografts, are ineffective when associated with comorbidities, in addition to complications such as organ rejection [5]. On the other hand, traditional wound care treatments such as medical bandages, wound dressings, debridement, hydrotherapy, and antibiotics primarily reduce the severity rather than promote wound healing. Therefore, there is an urgent need to explore alternative solutions that promote effective tissue regeneration.

Recent studies highlight the promise of natural bioactive compounds and biomaterials in enhancing wound healing and tissue regeneration [6,7]. Effective healing relies on coordinated processes, including inflammation, cell proliferation, extracellular matrix formation, and tissue remodelling. Natural compounds can support these processes by creating a bioactive environment that promotes tissue repair when incorporated into scaffolds or dressings. Manuka honey, rich in methylglyoxal, hydrogen peroxide, phenolics, and flavonoids, exhibits antimicrobial, antioxidant, and tissue-repair properties. It promotes fibroblast proliferation, angiogenesis, and collagen deposition, while its low pH and osmotic effects help maintain a moist, infection-resistant wound environment [8,9]. Fenugreek seeds contain flavonoids, alkaloids, saponins, and polysaccharides that provide antioxidant, anti-inflammatory, and antimicrobial effects. These compounds regulate inflammation, enhance fibroblast activity, support collagen synthesis, and improve moisture retention, all of which contribute to effective healing [10,11]. In addition to plant-derived compounds, the peptide hormone ghrelin shows strong therapeutic potential due to its anti-inflammatory and proangio-

genic properties [12]. It stimulates fibroblast proliferation and vascularisation, improving oxygen and nutrient delivery to healing tissues [13]. Because wound healing involves multiple biological pathways, targeting a single mechanism is often insufficient. Combining Ghrelin with natural bioactive compounds in biomaterial-based scaffolds or dressings offers a promising strategy to enhance tissue regeneration and improve wound-care outcomes.

One of the major challenges in wound healing is delivering therapeutic substances to the wound site and ensuring their stability. A potential solution to these challenges involves using engineered biodegradable polymeric scaffolds that mimic the native tissue. These scaffolds can be tailored to incorporate bioactive components, thereby enabling prolonged, targeted delivery and enhancing their therapeutic effects. Further, bioscaffolds enable interactions between cells and the extracellular matrix (ECM), which drive cellular behaviour and tissue formation [14,15]. Thus, creating a scaffold that replicates the *in vivo* architecture of the cells is likely to be beneficial for tissue regeneration [16]. Among several polymers, silk fibroin (SF), a natural protein polymer derived from the *Bombyx mori* silkworm [17], and polyvinyl alcohol (PVA) [18], a synthetic polymer known for its excellent nanofiber-forming ability, have been widely tested for their efficacy in wound healing. A recent study reported that nanosilver incorporated PVA fibres exhibit stable morphology and good biodegradability. These results underscore the PVA's suitability for advanced wound dressings [19]. Also, recent studies have shown that *Bombyx mori* silkworm fibroin (SF) can effectively filter blood toxins, demonstrating its potential as a promising hemosorbent [20,21]. Hence, combining these natural and synthetic materials into the composite scaffold will gradually increase its biological and thermochemical properties. Previous studies demonstrated that these biodegradable compounds promote accelerated wound healing, attributed to their enhanced degradation stability and excellent cytocompatibility [22,23].

In this study, we developed a PVA-SF blend nanofiber incorporating natural compounds (Manuka honey and Fenugreek seeds) and the peptide hormone Ghrelin. The scaffold was thoroughly characterized to confirm successful polymer blending, structural stability, and thermal behaviour. Scanning electron microscopy (SEM), Fourier transform infrared spectroscopy (FTIR), thermogravimetric analysis (TGA), and differential scanning calorimetry (DSC) were performed to study the structural and physicothermal properties of the scaffolds. *In vitro* assays were conducted to evaluate its antioxidant performance, angiogenic potential, and cytocompatibility toward skin-relevant cells. Together, these analyses demonstrate the potential of the developed bioscaffold to support and accelerate skin wound regeneration through a combination of antioxidant protection and enhanced vascularisation.

2. Materials and Methods

2.1 Materials

Polymers: PVA (molecular weight = 89,000–98,000), 99+% hydrolyzed, was purchased from Sigma-Aldrich, and SF was purchased from Xi'an Herbking Biotechnology (Gaoxin District, Xi'an, Shaanxi, China). The peptide hormone Ghrelin was obtained from Tocris (Batch number: 22a1463, Tocris Bioscience, Bristol, UK) and was kindly gifted by Prof Daryl Schwenke (University of Otago). Manuka honey was kindly gifted by ManukaMed (ref: MM0051C, Manuka Med (Gentell company), Masterton, Wellington region, New Zealand), and fenugreek seeds (Batch no: MZ/MF/23365, Indian Heritage, India) were purchased from the supermarket. Manuka honey was dissolved in the aqueous phase of fenugreek seed; Fenugreek seed powder and Ghrelin were dissolved in MilliQ water. All cell lines were validated by STR profiling and tested negative for mycoplasma.

2.2 Preparation of Polymer Solutions for Electrospinning

Polymer solutions for electrospinning were prepared by dissolving PVA and SF at various concentrations and ratios (70:30, 80:20, and 50:50, respectively) in MilliQ water. The mixtures were continuously stirred at 80–85 °C until a homogenous solution was achieved. As PVA is a temperature-sensitive polymer, the solutions were carefully monitored and maintained within this temperature range to preserve polymer stability and ensure reproducible electrospinning performance.

The final bioscaffold formulation used for electrospinning was prepared by dissolving 2.5 g of PVA and 2.5 g of Silk fibroin in 23 mL of MilliQ water. Subsequently, 2% Manuka honey, 20 µg of Ghrelin, and 2 mL of the aqueous phase of fenugreek seed extract phase were incorporated into the polymer solution to obtain a final volume of 25 mL. The selection of polymer concentrations and incorporation levels of the natural derivatives was primarily based on electrospinning feasibility, including stable jet formation, spinning duration, uniform fibre morphology, scaffold integrity, and overall biocompatibility, rather than on achieving a predefined therapeutic dose for a specific wound area. Preliminary electrospinning formulation trials were conducted to identify concentrations that ensured consistent jet stability and uniform nanofiber formation without bead defects (**Supplementary Figs. 1–3**). For the bioactive components, incorporation levels were guided by ranges reported in the literature that preserve biological activity while maintaining fibre uniformity [13,24,25].

2.3 Characterization of the Polymer Solution

The viscosity of the solutions with different ratios was measured using a Discovery Hybrid HR-3 Rheometer (TA Instruments, Newcastle, DE, USA) equipped with an MP61

liquid temperature control device at 20 °C, with cone-plate geometry (40 mm diameter and 1° angle), as described earlier [26].

2.4 Fabrication of Composite Bioscaffold

PVA-SF nanofiber scaffold and bioscaffold (combination of PVA-SF and natural compounds) were fabricated using an electrospinning device (TL-BM, Tong Li Tech Co., Ltd., Nanshan District, Shenzhen, Guangdong, China) with the following conditions: voltage ranging from 8–20 kV, needle to tip collector distance of 11–17 cm and flow rate between 1.2–2.5 mL/h. The parameters were decided following optimization using previously established parameters (**Supplementary Figs. 1–3**). A 22-gauge needle was used for spinning, and the whole process was carried out at room temperature. The nanofibrous scaffold was collected on aluminium foil wrapped around the collector. After fabrication, the scaffolds were stored in a desiccator until the assay.

2.5 Characterization of the Bioscaffold

2.5.1 SEM

The surface morphology of the PVA-SF and bioscaffold was examined using field emission scanning electron microscopy (JEOL 6700F FE-SEM, JEOL Ltd., Tokyo, Japan). Each scaffold was placed onto a double-sided carbon tape mounted on a metal stub prior to scanning; scaffolds were coated with a 10 nm layer of gold palladium in an Emitech K575X peltier-cooled high-resolution sputter coater (EM Technologies Ltd, Kent, England). Images were captured at 1000× and 10,000× magnifications. The diameters of the electrospun fibres were analyzed from SEM images using the ImageJ software V1.54s (NIH, MD, USA), (FIJI, NIH). Measurements were taken from 50 areas in each image.

2.5.2 Attenuated Total Reflectance Fourier Transform Infrared (ATR-FTIR) Spectroscopy

ATR-FTIR was used to confirm the presence of functional groups in the raw materials and scaffolds. Scaffolds measuring 1 × 1 cm^2 were directly placed on the machine (Alpha FT-IR, Bruker, MA, USA). Twenty scans were obtained for each FTIR spectrum in ATR mode. Data were acquired using Agilent resolution OPUS Pro^{TM} software (version 5.2.0, Bruker Optik, Ettlingen, Germany), and the spectra were baseline-corrected and smoothed using Origin Pro software (OriginLab, Version 2025b(10.25), MA, USA). All spectra were reported in the wavenumber range from 400–4000 cm^{-1}, with a spectral resolution of 4 cm^{-1}. Before data acquisition for each sample, a blank scan (without a sample) was performed and recorded to establish a baseline. Due to the extensive overlap of the major vibrational regions (O–H, N–H, and amide I/II) shared among PVA, SF, Manuka honey, and fenugreek seed extract, we did not perform peak deconvolution or curve-fitting analysis in our study. Instead, we employed well-established, more robust spectrum indicators, including characteristic peak shifts, band broadening, and functional group signatures, which are widely accepted for evaluating polymer-polymer and polymer-biomolecule interactions to distinguish component contributions [27,28].

2.5.3 Biodegradation Analysis

The degradation rate of the scaffolds was determined using the weight loss method. The scaffolds were cut into small circles of 8 mm diameter using a biopsy puncher (Miltex biopsy punch, Capes Medical, NZ). After recording the initial weight (W1) of the samples, they were placed in a test tube filled with 10 mL PBS and allowed to degrade for different time points (7, 14, 28 days). At each time point, the sample was removed, air-dried for 24 hours, and weighed again (W2). The percentage of scaffold degradation was calculated using the following equation.

$$\text{Degradation } \% = \frac{W1-W2}{W1} \times 100$$

2.5.4 Thermal Stability Assay—Thermal Stability of the Scaffolds was Assessed Using Two Techniques

2.5.4.1 TGA. TGA was performed to analyse the thermal stability and thermal decomposition of the prepared scaffolds and raw materials using a Q50 TGA analyser (TA Instruments, New Castle, DE, USA). The platinum sample pan (TA Instruments, DE, USA) was loaded with approximately 5–10 mg of sample and heated from 20 °C to 700 °C at a constant heating rate of 10 °C/min under a N_2 supply at a flow rate of 20 mL/min. The TRIOS software (TA Universal Analysis 2000 V4.OC, TA Instruments) was used to obtain the data, and OriginPro software (OriginLab, Version 2025b(10.25), MA, USA) was used to analyze and plot the graphs.

2.5.4.2 Differential Scanning Calorimetry (DSC). The thermal responses of pure PVA, SF, Manuka honey, fenugreek seeds, and scaffolds were determined using a Q1000 differential scanning calorimeter (TA Instruments, New Castle, DE, USA). Approximately 2–6 mg of each sample was weighed into a standard aluminium DSC pan and crimped with a pin-holed standard aluminium lid. The samples were heated from 10 to 300 °C at a controlled rate of 10 °C/min under a dynamic nitrogen atmosphere of 50 mL/min. The DSC data were analyzed using TA Universal Analysis 2000 V4.OC software and OriginPro software were used to analyze and plot the graphs.

2.5.4.3 *In Vitro* Release Studies. To determine the *in vitro* cumulative release behaviour of the electrospun bioscaffolds, 10 mg of bioscaffold was immersed in 3 mL of PBS (pH 7.4) and incubated at 37 °C under gentle shaking to simulate physiological conditions. The release medium (0.3 mL) was withdrawn at predetermined time intervals and replaced with an equal volume of fresh PBS. The amount

of released bioactive compounds was determined using UV-visible spectrophotometry at the predetermined wavelengths of 310 nm and 330 nm corresponding to the loaded components. The release concentration at each time point (C_t) was calculated from the calibration curve of standard solutions. All measurements were performed in triplicate.

2.6 Antioxidant Assay

The intrinsic antioxidant property of the nanofibrous scaffolds was evaluated using the 1,1-diphenyl-2-picrylhydrazyl (DPPH) assay (Sigma-Aldrich, Molecular weight 394.32 Da). Briefly, a 0.2 mM DPPH solution was prepared by dissolving 7.88 mg of DPPH powder in 100 mL of 99% methanol. For the assay, 5 mg of each scaffold sample was mixed with 1.5 mL of the prepared DPPH solution and incubated at room temperature. The absorbance of the mixture was recorded at 517 nm using a microplate reader (SpectraMax® i3X, catalog number: MDMR-004, CA, USA) at 24 and 48 hours. The DPPH radical scavenging activity was calculated using the following equation:

$$\text{DPPH}\ (\%) = (A_{control} - A_{sample}) / A_{control} \times 100$$

where $A_{control}$ is the absorbance of DPPH radical in methanol, and A_{sample} is the absorbance of DPPH radical plus sample extract.

2.7 Cytotoxicity Study

The cytotoxicity of the scaffold was evaluated using the human umbilical vein endothelial cell line (HUVECs, Thermo Fisher Scientific Limited, New Zealand) and the human keratinocyte cell line (HaCaT, ATCC® CRL-2404) using the CellTiter 96® non-radioactive cell proliferation assay Kit (3-(4,5-dimethylthiazol-2-yl)-2,5-diphenyltetrazolium bromide (MTT), Promega Corporation, Madison, WI, USA). HUVECs were cultured in endothelial basal medium (M200, ThermoFisher), supplemented with a low serum growth supplement (ThermoFisher), 10% Fetal bovine serum (FBS), and 1X Antibiotic-Antimycotic (ThermoFisher). HaCaT cells were cultured in Dulbecco's Modified Eagle medium (DMEM), supplemented with 10% FBS and 1X Antibiotic-Antimycotic (ThermoFisher). Both cell lines were maintained at 37 °C, 5% CO_2, and 95% humidity. For the assay, cells were seeded at a concentration of 10,000 cells/well in 100 µL of complete growth medium in a sterile 96-well flat-bottomed plate (Falcon plate, Corning Coster, USA) and incubated at 37 °C for 24 hours to allow for cell adherence. The following day, 8 mm UV-treated (30 min) scaffolds (PVA-SF scaffold or bioscaffold) were placed directly into the wells and the cells were cultured for an additional 72 hours. For this study, cytotoxicity was monitored only up to 72 hours, a widely recognized standard time point for evaluating acute cell viability on biomaterials [29].

This duration was sufficient to assess the initial biocompatibility and detect any immediate cytotoxic effects of the scaffold components, including PVA, SF, and the incorporated bioactive compounds. Cells without a scaffold served as the control. At the conclusion of the treatment period, the growth media were carefully removed, and cells were gently washed three times with PBS (PH 7.4). Next, 100 µL of PBS and 15 µL of MTT solution were added to each well, followed by a 4-hour incubation at 37 °C. The reaction was then stopped by adding a stop solution, followed by incubation for an additional 1 hour. Afterwards, the absorbance was measured at 570 nm using a microplate reader (SpectraMax® i3X). The MTT assay was performed in triplicate across three independent scaffolds, and cell viability was expressed as a percentage of viable cells relative to the negative control.

2.8 Scratch Assay

A scratch assay was conducted to determine the effect of the scaffold on HUVEC migration, as a measure of *in vitro* wound-healing properties. For this experiment, HUVECs were plated at 50,000 cells/well in complete M200 medium into a 24-well plate coated with fibronectin and cultured for 48 hours until the cells reached 90% confluence. Using light pressure, a scratch was created on the monolayer of cells in each well with the sharp end of a 200 µL pipette tip. The cells were then washed twice with PBS to remove cellular debris and replaced with fresh FBS-free M200 medium to ensure the observed wound closure was due to migration rather than proliferation. Subsequently, cell culture inserts with the scaffold and 300 µL FBS-free M200 media were placed on top of the well. Serial images were captured at baseline (time 0) and at 4, 8, 12, 16, and 24 hours after the scratch to monitor cell migration. The images were analyzed using the Wound-Healing Size Tool plugin in FIJI (NIH) to calculate the area not covered by cells. The wound area at each time point is expressed as a percentage of the initial area (time 0), eliminating bias from scratches of varying sizes.

The scratch area at each time point was measured using ImageJ software V1.54s (NIH, MD, USA), and the percentage of wound closure was calculated according to the following formula:

$$\text{Wound Closure}(\%) = \frac{\text{Initial Scratch Area} - \text{Scratch Area at Time (t)}}{\text{Initial Scratch Area}} \times 100$$

Initial scratch area is time 0 h, scratch area at time t – (4, 8, 12, 16, 20, and 24 h).

2.9 Cell Proliferation on Scaffold

The scaffold's efficacy in promoting cell growth was determined using the cardiomyocytes (AC-16) cell line. AC-16 are immortalized human ventricular AC-16 received from Dr Mercy Davidson of Columbia University (Institutional Review Board approval (IRB#X0592) [30]. AC-16 cells are widely used to study cellular interactions and responses to biomaterials and oxida-

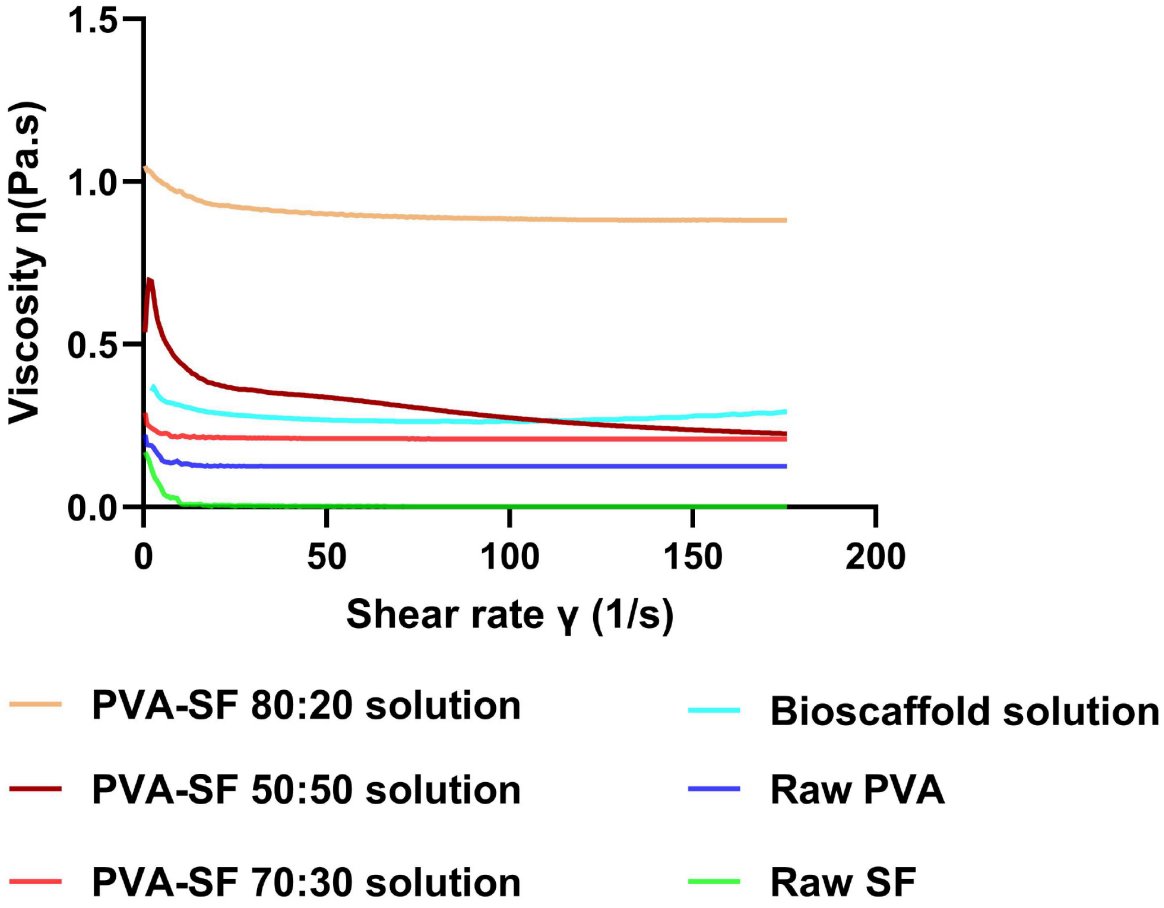

Fig. 1. Rheology analysis of the spinning solution. The viscosity graph of Raw PVA, Raw SF and PVA-SF at ratios of 70:30, 80:20, PVA-SF 50:50, and after incorporating the natural components (bioscaffold). The PVA-SF 50:50 ratio and bioscaffold solution exhibited a non-Newtonian fluid behaviour, while other preparations exhibited Newtonian fluid behaviour. In the viscosity graphs, the X-axis represents the shear rate, and the Y-axis represents the viscosity. PVA, polyvinyl alcohol; SF, silk fibroin.

tive stress [31]; hence, we used AC-16 cells for our study. AC-16 cells were cultured in DMEM supplemented with 10% FBS and 1% antibiotic-antimycotic. Once the cells reached confluency, 1×10^6 cells were labelled with CellTracker dye CM-1,1′-Dioctadecyl-3,3,3′,3′-Tetramethylindocarbocyanine Perchlorate (DiI) (C7000, Molecular Probes) according to the manufacturer's instructions. A pre-sterilized scaffold was placed on cover glasses using Histoacryl Blue Tissue Adhesive (Capes), followed by seeding 10,000 cells onto the scaffold. Images were captured at different time intervals using the EVOS 5000 fluorescence microscope. ImageJ (NIH, USA) was used to quantify the cell population.

2.10 Statistical Analysis

All the experiments were carried out in triplicate in different regions on 3 independent scaffolds, and the data were expressed as the mean ± standard deviation (SD). The data distribution was assessed using the Shapiro-Wilk normality test. Statistical analysis was performed using either a one-way Analysis of Variance (ANOVA) or a two-way ANOVA with Tukey's post hoc test in GraphPad Prism (GraphPad Software, LLC, version 9.5.1, Boston, MA, USA). p values < 0.05 were considered to be statistically significant.

3. Results

3.1 Successful Fabrication and Characterization of Bioscaffolds

3.1.1 Optimal Viscosity of the Electrospinning Solution

The viscosity of the spinning solution determines the surface morphology, defect-free, and continuous formation of the nanofiber. Hence, the rheological behaviour of the polymer solutions composed of PVA and SF at different ratios, with and without the addition of natural components (Manuka honey, fenugreek seed, Ghrelin), was investigated using a rheometer. As shown in Fig. 1 and **Supplementary Fig. 4**, rheological analysis revealed that the PVA-SF 50:50 formulation exhibited more pronounced non-Newtonian behaviour than the other PVA-SF ratios, as reflected by changes in viscosity with increasing shear rate. Different ratios (70:30, 50:50, 80:20) showed a mixture of

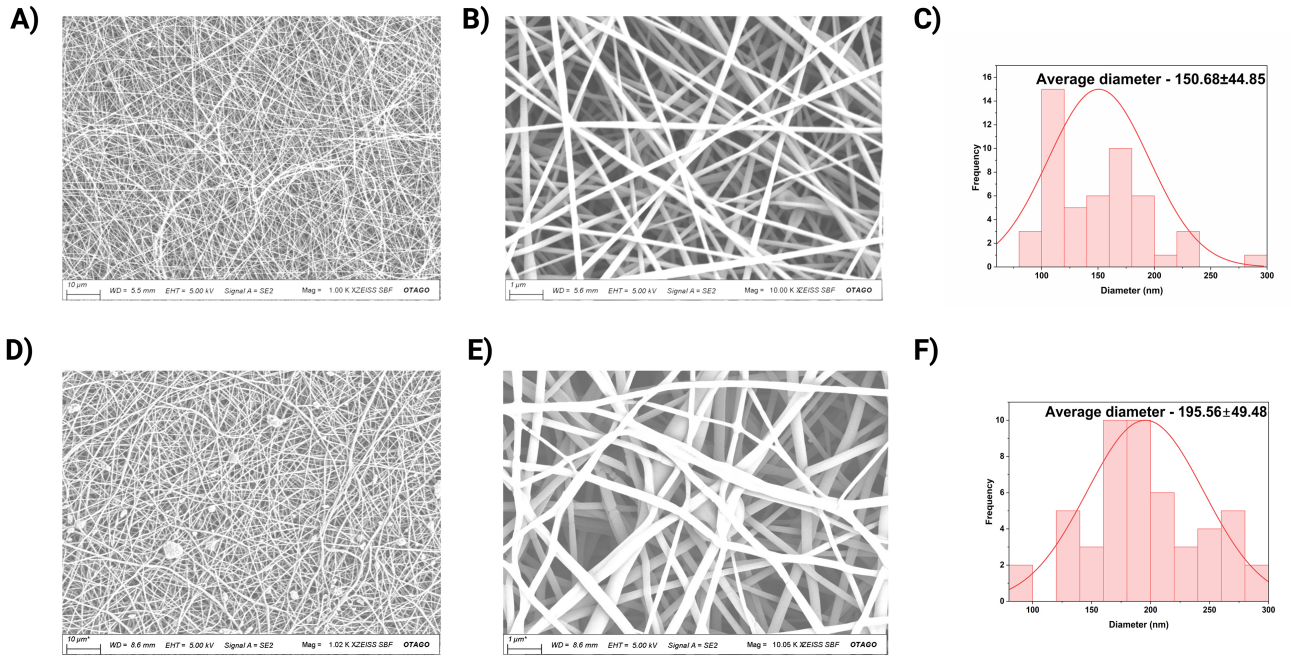

Fig. 2. SEM analysis of the electrospun nanofibrous scaffolds. (A,B,D,E) Representative SEM images of PVA-SF (A,B) and bioscaffold (D,E). Panels (A) and (D) display images at 1000× magnification (scale bar: 10 µm), while (B) and (E) are at 10,000× magnification (scale bar: 1 µm). Panel (C,F) represents a distribution bar graph illustrating the nanofiber diameters: PVA-SF fibres have an average diameter of 150.68 ± 44.85 nm (C), while the bioscaffold fibres have an average diameter of 195.56 ± 49.48 nm (F). SEM, Scanning Electron Microscopy.

high and low viscosity, depending on their composition. Among these, the PVA-SF 80:20 blend showed the highest viscosity of 1.05 Pa · s, which is likely to hinder stable jet formation due to its high resistance, leading to the development of defects in the fibres during electrospinning. Conversely, the PVA-SF 70:30 ratio showed a lower viscosity of 0.25 Pa·s, potentially leading to the formation of thin fibres or bead formation due to insufficient chain entanglement. The PVA-SF 50:50 ratio exhibited an optimal viscosity profile, characterized by moderate flow resistance while maintaining the desired shear-thinning properties, enabling stable jet formation and uniform fibre deposition. Therefore, this composition was selected as the most suitable ratio for electrospinning. While there was a small reduction in viscosity upon incorporation of bioactive compounds, it remained within the acceptable spinning range. Overall, these results confirm that the formulated PVA-SF 50:50 ratio, well balanced between viscosity and shear thinning behaviour, is key to achieving a uniform and defect-free PVA-SF scaffold and a natural components incorporated bioscaffold.

3.1.2 Successful Fabrication of Bioscaffold

The SEM analysis of the fabricated bioscaffold confirmed the absence of any major or minor defects apart from minimal nanoscale defects (Fig. 2A,B,D,E and **Supplementary Figs. 5,6**). Quantitative analysis confirmed the fibre diameter of PVA-SF scaffold was in the range 150.68 nm ± 44.85 (Fig. 2C). Upon incorporation of the natural compounds, the average fibre diameter increased to 195.56 ± 49.48 nm (Fig. 2F). This size of the nanofibers are favourable in mimicking the native ECM and enhancing cell-scaffold interactions to promote cell growth, differentiation and proliferation [32–34]. Moreover, the slightly increased fibre diameter in the natural compound-loaded scaffold may improve retention and localized availability of antioxidant and proangiogenic compounds. This structural feature can facilitate sustained interaction of the incorporated natural components with surrounding cells, potentially enhancing free-radical scavenging activity and promoting endothelial cell migration.

3.2 ATR-FTIR Spectroscopy of the Bioscaffold Confirmed the Presence of PVA, SF, Manuka Honey and Fenugreek Seed Functional Groups

FTIR was used to analyze the chemical interaction of the polymers and to identify the incorporated natural components in the composite matrix (Fig. 3 and individual repeats in **Supplementary Fig. 7**). Raw Fenugreek seed powder (Fig. 3A) showed its characteristic peak at 3365 cm^{-1} due to the N–H stretching, followed by a small peak at 2927 cm^{-1} corresponding to C–H stretching. The appearance of strong peaks at 1657 and 1544 cm^{-1} denotes the presence of C=O (amide I), and N–H (amide II) [35].

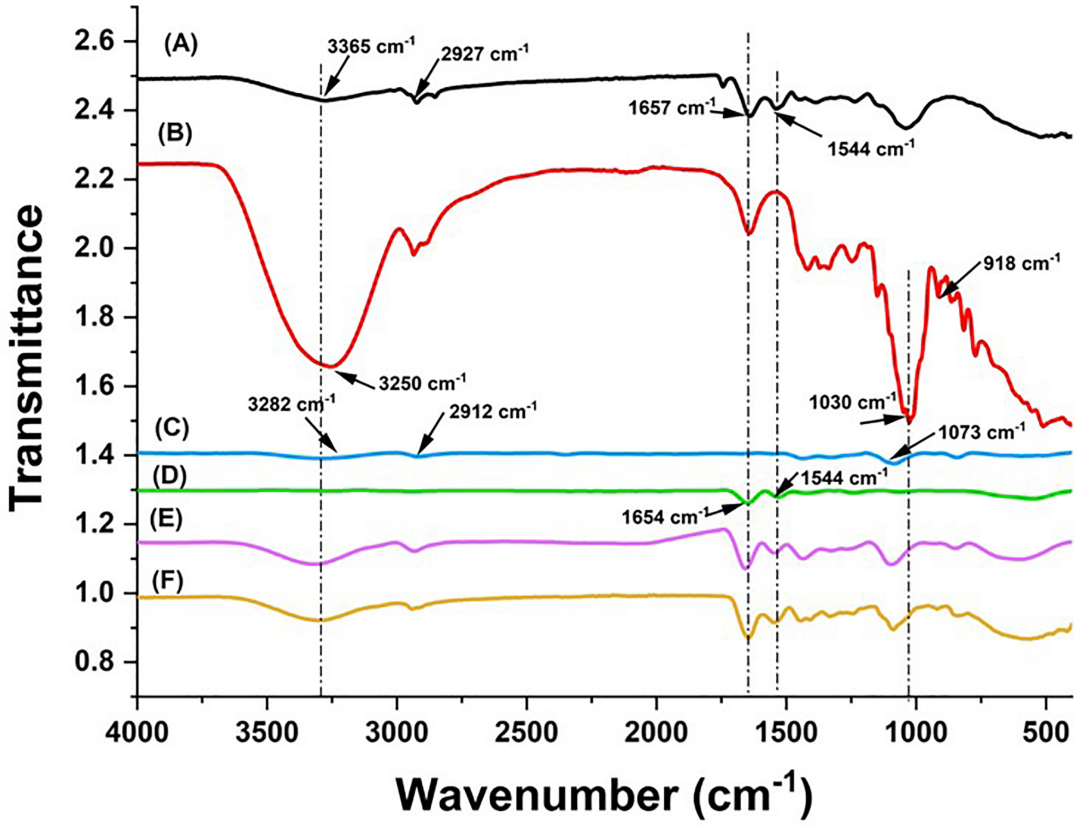

Fig. 3. ATR-FTIR spectroscopy analysis of the electrospun nanofibrous scaffolds. (A) Raw Fenugreek seeds, (B) Raw Manuka honey, (C) Raw PVA, (D) Raw SF, and an overlaid comparison with the (E) PVA-SF composite and (F) bioscaffold. In the PVA-SF spectrum, notable shifts occur at peaks 3282, 1654, and 1544 cm^{-1}, which correspond to the O–H group, amide I, and amide II, respectively. In the bioscaffold, shift changes occur at amide I, amide II, and 1030 cm^{-1}, which corresponds to C–O stretching (sugar group). The spectra span 400–4000 cm^{-1}, with the x-axis representing wavenumber (cm^{-1}) and the y-axis indicating percentage transmittance. ATR-FTIR, Attenuated Total Reflectance-Fourier Transform infrared Spectroscopy.

Raw Manuka honey (Fig. 3B) showed a broad peak at 3250 cm^{-1}, denoting O–H stretching. A sharp, dominant peak at 1030 cm^{-1} corresponds to C–O (glucose). A small peak at 918 cm^{-1} corresponds to the C–H bending., and the bands from 900–750 cm^{-1} indicate the stretching of C–O and C–C [36]. Raw PVA (Fig. 3C) showed four major peaks at 3282 cm^{-1} (O–H stretching), 2912 cm^{-1} (asymmetric stretching of CH_2), 1430 cm^{-1} (CH_2 bending), and 1073 cm^{-1} (stretching of C=O). While raw SF showed the peaks at 1654 cm^{-1} (amide I, C=O stretching) and 1544 cm^{-1} (amide II, N–H bending), indicating the presence of β-sheet structure in SF (Fig. 3D). In addition, two other peaks were observed at 1232 cm^{-1} (amide III, C–N stretching, assigned to the random coil conformation) and 3269 cm^{-1} (N–H stretching).

Following the blending of PVA into the SF, the FTIR spectrum of PVA-SF scaffold (Fig. 3E) exhibited the characteristic bands of both PVA and SF, confirming their effective intermolecular interactions. Specifically, we observed a slight shift in the position of amide I to 1654 cm^{-1} upon blending it with PVA. This suggests a strong interaction between the PVA hydroxyl group and the amide groups in the SF. Noticeably, the width of the O–H region (3300–3200 cm^{-1}) broadened in the PVA-SF spectrum. This indicates an increase in hydrogen bonding between the O–H groups of PVA and the C=O groups of SF. Further, the absence of new peaks indicates the uniform blending of PVA-SF polymers. All peaks observed were consistent with the published literature [37,38].

The electrospun bioscaffold spectrum (Fig. 3F) retained all the major characteristic peaks corresponding to the polymers and the incorporated natural compounds. Notably, the amide I band exhibited a slight shift to 1651 cm^{-1} compared with the PVA-SF scaffold spectrum, indicating interactions between the hydrogen-bonding networks of the polymers and the incorporated Manuka honey and fenugreek seed extract. This shift confirms the presence of secondary intermolecular interactions between silk fibroin and the natural bioactive components within the nanofiber matrix. The characteristic C–O stretching of Manuka honey 1030 cm^{-1} and N–H stretching of fenugreek seed 3365 cm^{-1} were faintly shifted to 1075 cm^{-1} and 3345 cm^{-1}, re-

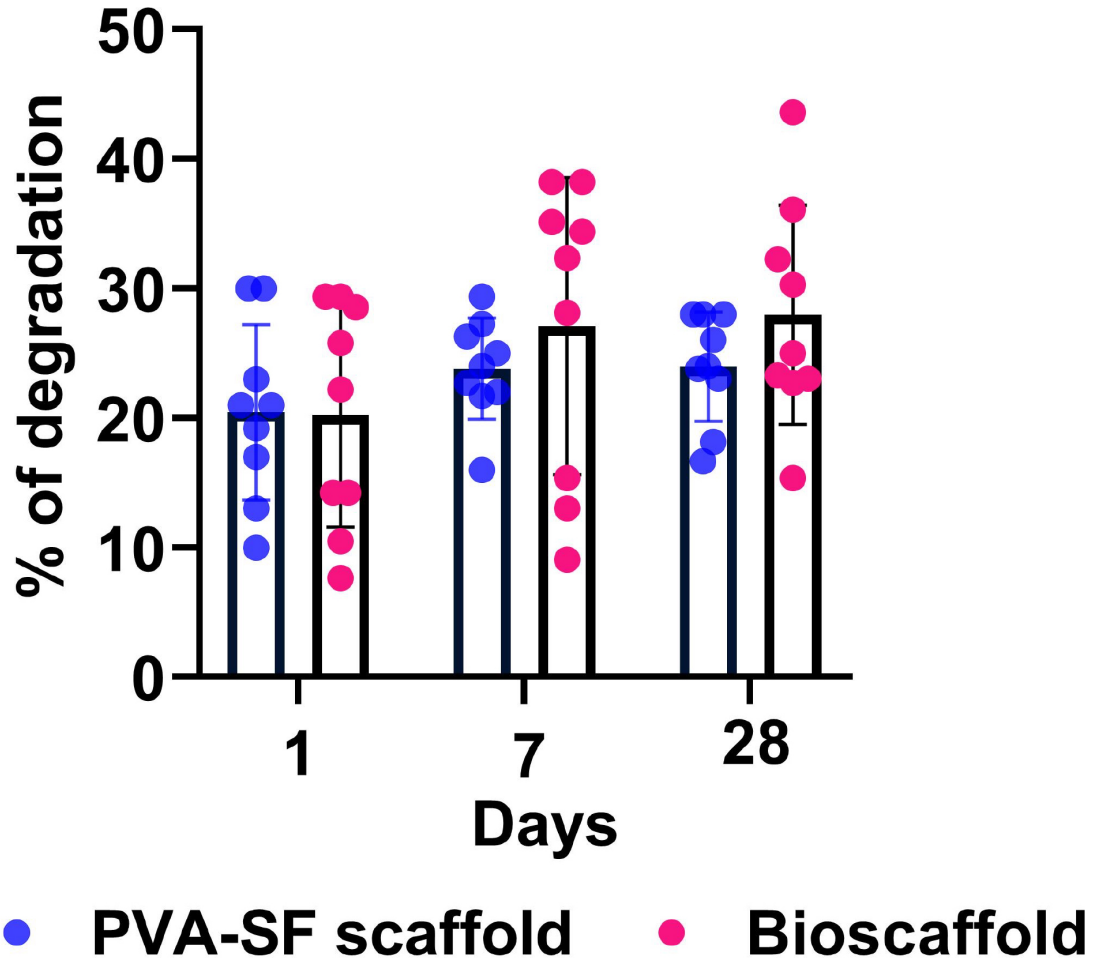

Fig. 4. Degradation analysis of the electrospun nanofibrous scaffolds. Quantitative scatter plot bar graphs showing degradation of PVA-SF scaffold and bioscaffold on day 1, 7, and 28. Data are represented as mean degradation percentage ± SD at various time points, analyzed using one-way ANOVA. There is no statistical difference observed. Experiments were performed in triplicate across different regions of a scaffold and repeated with 3 individual scaffolds. ANOVA, Analysis of Variance; SD, Standard Deviation.

spectively, suggesting a slight overlap of hydrogen bonding between the composites and with the N–H groups present in the fenugreek seed. Despite minimal shifts relative to the raw materials, the presence of characteristic peaks in the bioscaffold confirms a good interaction among the different materials within the scaffold.

3.3 Sustained and Slow Degradation of Bioscaffold

For wound-care applications, an ideal scaffold should degrade gradually while preserving its architecture, thereby supporting tissue repair and enabling controlled release of incorporated bioactive components to achieve optimal therapeutic outcomes. In the present degradation analysis, no statistically significant difference in weight loss was observed between the two scaffold groups (Fig. 4). However, the bioscaffold showed a comparatively higher weight loss at day 7, likely attributable to the hydrophilic nature of the incorporated natural compounds. This early weight loss suggests an initial release of bioactive components from the PVA-SF matrix, which may accelerate early-stage wound-healing responses. Beyond the first week, the degradation rate stabilized for both scaffold groups, with overall degradation remaining below 30% by day 28, indicating sustained structural integrity and a slow, controlled degradation profile.

3.4 Bioscaffolds are Thermally Stable

3.4.1 TGA

A thermal analysis of the nanofibers is essential to evaluate their thermal stability and moisture degradation rate, and to identify the thermal decomposition of the individual materials used. In wound care applications, thermal stability is important for quantifying scaffolds' stability, which is required to support tissue repair and regeneration; it also helps predict the material's longer-term *in vitro* and *in vivo* degradation behaviour and performance.

The thermogram of all the raw materials showed an initial weight loss occurring between 80–150 °C, attributed

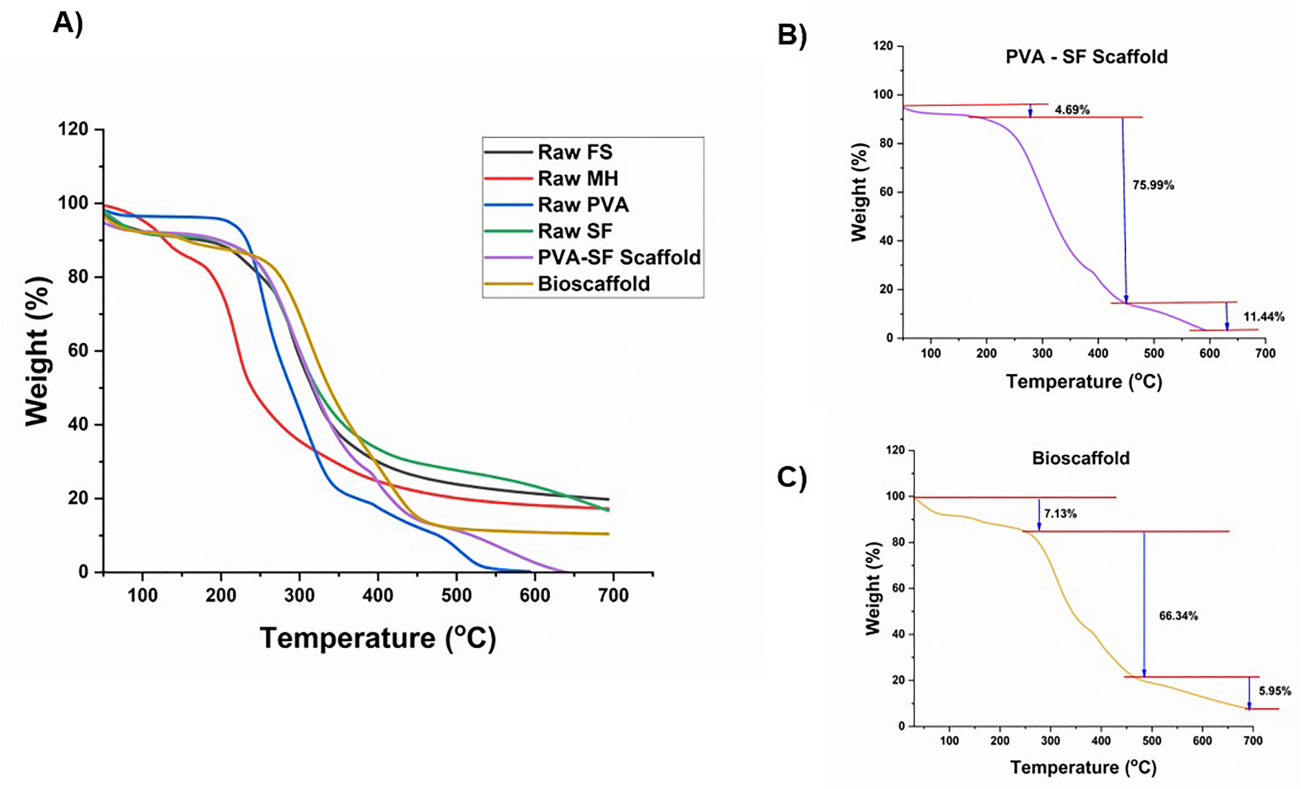

Fig. 5. Thermal analysis of the electrospun nanofibrous scaffolds. Representative TGA thermogram of Raw Fenugreek seed, Manuka honey, PVA, SF, PVA-SF, and bioscaffolds composites. (A) Raw samples and scaffolds, (B) PVA-SF scaffold, (C) bioscaffold. The X axis represents the temperature (°C), and the Y axis represents the percentage of weight loss. TGA, Thermogravimetric Analysis.

to the evaporation of moisture present in the hydrophilic polymers and the natural components. Subsequently, the thermal degradation of natural components occurred in the range of 220–350 °C, corresponding to the decomposition of carbohydrates, lipids, and sugar molecules inherent in these materials (Fig. 5A and individual repeats in **Supplementary Fig. 8**) [39–41].

The initial degradation of the PVA-SF scaffold occurred at 150 °C, resulting in a weight loss of 4.69%. A subsequent significant degradation occurred between 250 °C and 300 °C, due to the breakdown of polymer chains including amino groups, vinyl groups, and C–C bonds within the SF and PVA backbones (Fig. 5B) [42–44]. Beyond 600 °C, the TGA curves plateaued, indicating that the composite nanofibers had fully decomposed, leaving little to no unburned inorganic residue. The decomposition temperature of the PVA-SF composite lies between that of raw SF and PVA, possibly due to an increase in crystallinity during the electrospinning process. Bioscaffolds showed an initial degradation at around 150 °C, resulting in a weight loss of approximately 7.13%. This suggests the presence of new, additional materials. The second decomposition of the bioscaffolds occurred around 270 °C, resulting in a weight loss of approximately 66.36%, which was 9.65% less than the PVA-SF scaffold (Fig. 5C). These findings indicate that the incorporation of new natural compounds enhanced the thermal stability of the bioscaffolds, potentially enhancing their flexibility and resistance to brittleness [45]. Such stability is beneficial for wound-healing applications, as it supports sustained bioactive delivery and helps maintain the scaffold's structural integrity throughout the tissue-regeneration process.

3.4.2 Differential Scanning Calorimeters (DSC)

The glass transition temperature (T_g) of raw fenugreek seed was 80 °C, corresponding to protein denaturation and water loss [25,46]. In the case of raw Manuka honey, two thermal events were exhibited; T_g was observed around 118 °C (Fig. 6A and individual repeats in **Supplementary Fig. 9**), followed by an endothermic peak around 220 °C, corresponding to the transition of amorphous sugar matrix, such as fructose or glucose, which are the major components of Manuka honey [40,41].

The T_g curves of PVA and SF were observed between 75 and 95 °C, indicating the release of water. This is followed by an endothermic peak between 225 °C and 240 °C, denoting the breakdown of amorphous amide groups in SF and the melting of crystalline domains in PVA [47–49].

Analysis of the PVA-SF scaffold curve (Fig. 6B) showed a visible shift in the T_g to 90 °C, indicating intermolecular interactions between PVA and SF. Interestingly, T_g of bioscaffold was around 120 °C, 30% higher when

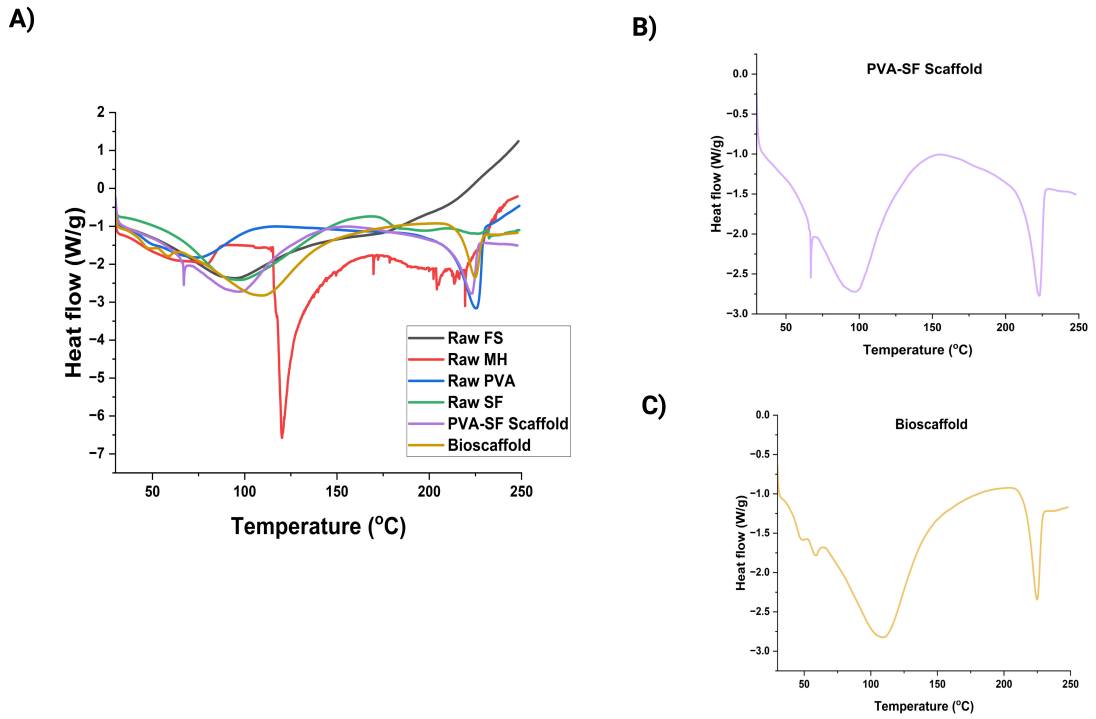

Fig. 6. DSC thermogram analysis of the electrospun nanofibrous scaffolds. Representative trace of DSC thermogram of Raw fenugreek Seed, Manuka honey, PVA, SF, PVA-SF, and bioscaffold (A), PVA-SF scaffold (B) and bioscaffold (C). The X-axis represents the temperature (°C), and the Y-axis represents the heat flow. DSC, Differential Scanning Calorimetry.

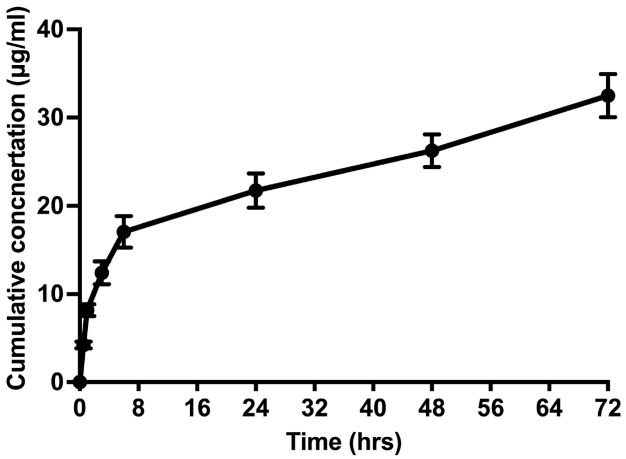

Fig. 7. Drug delivery analysis of the electrospun bioscaffolds. Quantitative line graph showing the cumulative release kinetics of natural compounds incorporated into bioscaffolds. Data presented as µg/mL and are presented as mean ± SD, n = 3 independent scaffolds with three technical repeats in each scaffold.

compared to the PVA-SF composite (Fig. 6C). Further, the thermal decomposition of the PVA-SF was around 217 °C, which increased to 227 °C after incorporation of natural compounds, indicating that the addition of natural derivatives enhances the overall thermal stability.

3.5 Bioscaffolds Release Active Compounds

The scaffold exhibited a sustained and time-dependent cumulative release pattern over 72 h. An initial burst of release was observed at early time points, reaching 17.0 ± 1.8 µg/mL at 6 h (Fig. 7). This is likely due to rapid leaching of surface-bound bioactive compounds from the nanofibers. This early release is beneficial for wound healing, as the immediate availability of Manuka honey and fenugreek phytochemicals can provide antimicrobial, anti-inflammatory, and antioxidant effects at the wound site. Following the initial phase, the bioscaffold demonstrated a controlled and sustained release profile, with cumulative release reaching 26.2 ± 1.9 µg/mL at 48 h and 32.5 ± 2.4 µg/mL at 72 h (Fig. 7). This sustained release is likely due to the gradual release of encapsulated compounds from the nanofibrous matrix's inner structure.

3.6 Functional Efficacy of the Bioscaffold

3.6.1 Bioscaffold Was not Cytotoxic

The cytotoxicity of the bioscaffold was assessed using the MTT colourimetric assay. Both PVA-SF and bioscaffolds showed no changes in cell viability for HUVECs and HaCaTs cells (Fig. 8). Over the incubation period of 72 hrs, all the scaffold groups showed no sign of cytotoxicity, confirming that nanofibers are non-toxic and biocompatible. Specifically, the absence of cytotoxic responses demonstrates that the fabricated scaffolds can act as drug

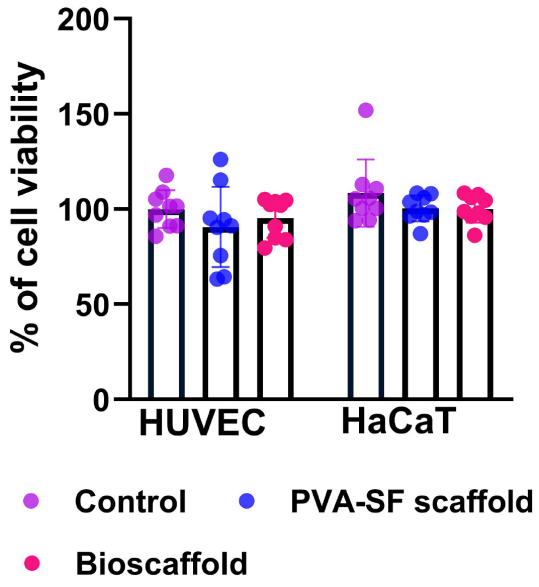

Fig. 8. Toxicity analysis of the electrospun nanofibrous scaffolds. Quantitative scatter plot bar graphs showing the effect of nanofibrous scaffolds on the viability of HUVECs and HaCaTs cells. Cell viability was measured 72 hours after the scaffold was added to the cells. Data are represented as mean ± SD and analyzed using one-way ANOVA. There is no statistical difference observed. Experiments were done in triplicate and repeated on 3 individual scaffolds. HUVECs, Human Umbilical Vein Endothelial Cell line; HaCaTs, Human adult calcium-low Temperature-tolerant keratinocytes.

delivery systems and provide a supportive microenvironment for effective cell proliferation, thereby accelerating wound repair [50].

3.6.2 Bioscaffold Improved Migration of HUVECs

The scratch assay was used to demonstrate the angiogenic potential of bioscaffolds, which are an essential requirement for effective wound care dressings. Effective cell migration is a critical step in wound repair, as it facilitates revascularisation and nutrient delivery and promotes better regeneration. The PVA-SF scaffold demonstrated better migration rates at 8 hours (p = 0.019) and 12 hours (p = 0.025) compared to bioscaffold-treated cells. However, bioscaffold-treated cells showed better migration (91 ± 9.1%) at 24 hours compared to control (68.55 ± 8.4%, p < 0.0001) and PVA-SF (79.07 ± 9.7%, p = 0.049) (Fig. 9 and individual repeats in **Supplementary Figs. 10.1–10.8**).

3.6.3 Bioscaffold Supports the Proliferation of Cells

The efficacy of the bioscaffold in supporting cell growth and proliferation was determined using DiI-labelled AC-16 cells. Fluorescence images demonstrated both PVA-SF and bioscaffold supported the proliferation of cells over the cultured period (Fig. 10A). Further quantification on AC-16 cells cultured on the bioscaffold confirmed better growth on bioscaffold compared to other groups (Fig. 10B). Notably, the cells displayed a well-defined elongation and spreading morphology, indicating that the nanofibers successfully mimic the ECM, thereby providing the required microenvironment for the cells to attach and grow.

3.6.4 Bioscaffolds Exhibit Better Antioxidant Potential

The antioxidant capacity of the scaffolds was evaluated using the DPPH radical-scavenging assay. Both the PVA-SF scaffold and the bioscaffold exhibited antioxidant activity (Fig. 11). The bioscaffold demonstrated the highest free DPPH radical scavenging activity at both 24 (47.24 ± 9.2%) and 48 hours (67.59 ± 7.68%) compared to the PVA-SF scaffold, which showed 25.22 ± 6.08% and 37.68 ± 7.15% scavenging activity at 24 and 48 hours, respectively (p < 0.00001 at both time points).

4. Discussion

Tissue repair and regeneration are dynamic and complex process that requires the coordinated activity of growth factors, ECM components, and both resident and recruited cells. The ECM provides a structural and biochemical scaffold that is essential for cell adhesion, proliferation, migration, and differentiation, thereby guiding effective tissue regeneration [51]. In this study, we successfully fabricated a composite bioscaffold integrating synthetic PVA with natural components such as silk fibroin, Manuka honey, fenugreek seed extract, and Ghrelin. This integration aims to leverage the complementary properties of these materials for wound healing and broader biomedical applications. Wound healing is often impaired by excessive ROS [52], chronic inflammation [53], and inadequate angiogenesis [54]. The natural additives selected for this study, Manuka honey, fenugreek seed extract, and Ghrelin, were chosen specifically to address these barriers. Manuka honey is well documented for its antibacterial and anti-inflammatory effects [55–57], fenugreek seeds are known for their antioxidant and collagen-promoting properties [25], and Ghrelin is recognized for its proangiogenic and cytoprotective effects [58,59]. By successfully embedding all three natural additives within a nanofibrous PVA-SF matrix, we aimed to achieve a synergistic, multi-modal therapeutic effect.

Our optimization of the electrospinning process produced nanofibers with diameters less than 200 nm, which are favourable for mimicking the native ECM and enhancing cell-scaffold interactions to promote cell growth, differentiation, and proliferation [32–34]. SEM analysis confirmed that the fibres were uniform and defect-free. The slight increase in the diameter of the bioscaffold fibres is likely due to changes in viscosity resulting from the incorporation of the natural additives. FTIR spectra indicated successful blending, with minor shifts in functional group peaks suggesting molecular interactions between the polymer matrix and the bioactive compounds. Physicochemical assessments demonstrated that the bioscaffold

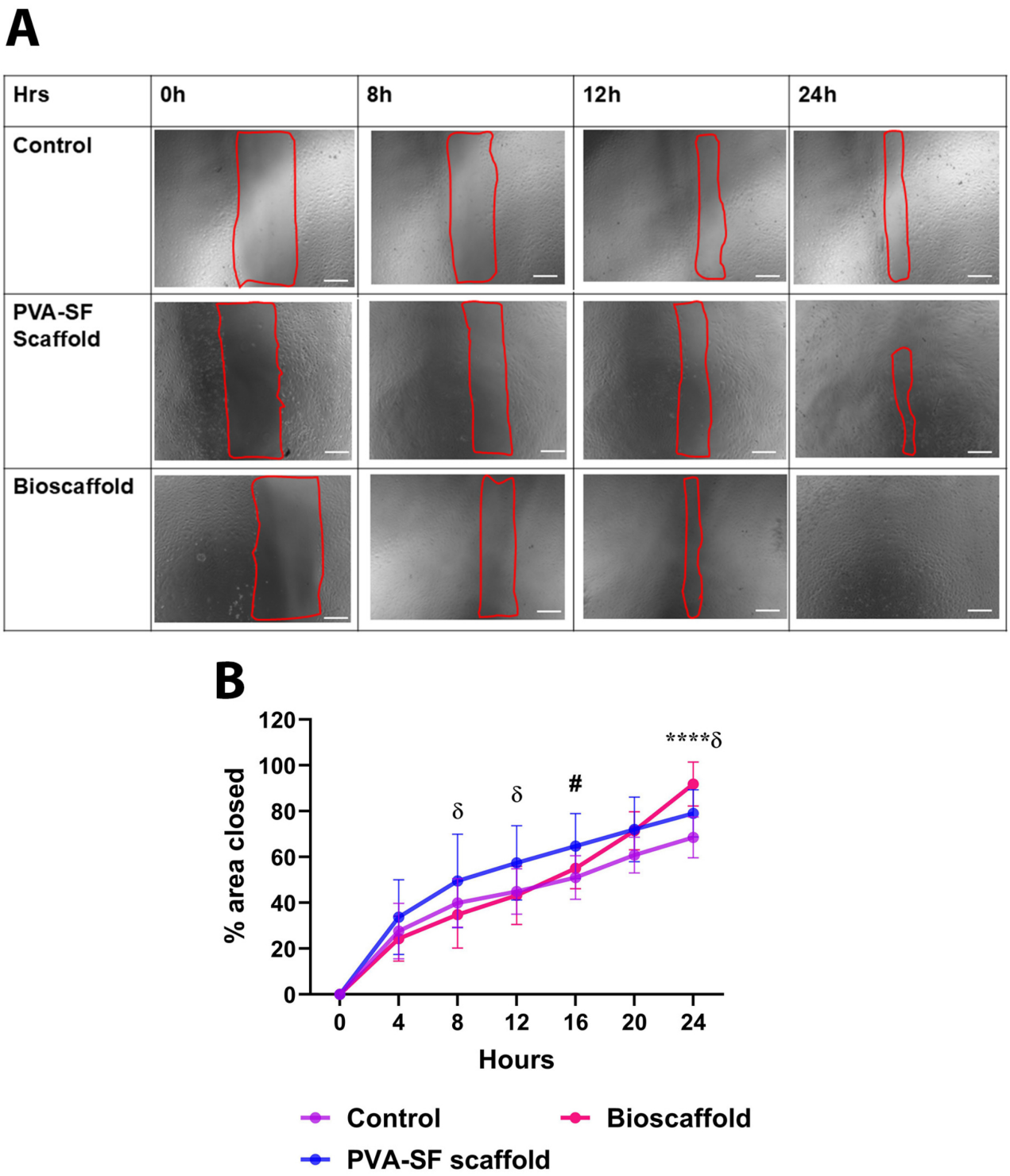

Fig. 9. Wound healing analysis of the electrospun nanofibrous scaffolds. (A) Representative bright-field microscopic images showing HUVEC migration at different time points. Images were captured at 4× magnification. The red box indicates the wound area. Scale bar is 750 µm. (B) Quantitative line graph showing the area of scratch closed as a percentage over a period of 24 hours. Quantitative line graph shows wound closure over time. Data are presented as the percentage of wound area and as mean ± SD. Differences were compared using a two-way ANOVA, followed by Tukey's multiple comparisons test. Experiments were conducted in triplicate and repeated with three independent scaffolds. Control cells without any scaffold; Bioscaffold—a combination of PVA-SF and natural compounds. ****$p < 0.0001$, control vs. bioscaffold; #$p = 0.0334$, control vs. PVA-SF scaffold; $\delta p = 0.0196$ at 8 hours, $p = 0.025$ at 12 hours and $p = 0.049$ at 24 hours, PVA-SF scaffold vs. bioscaffold.

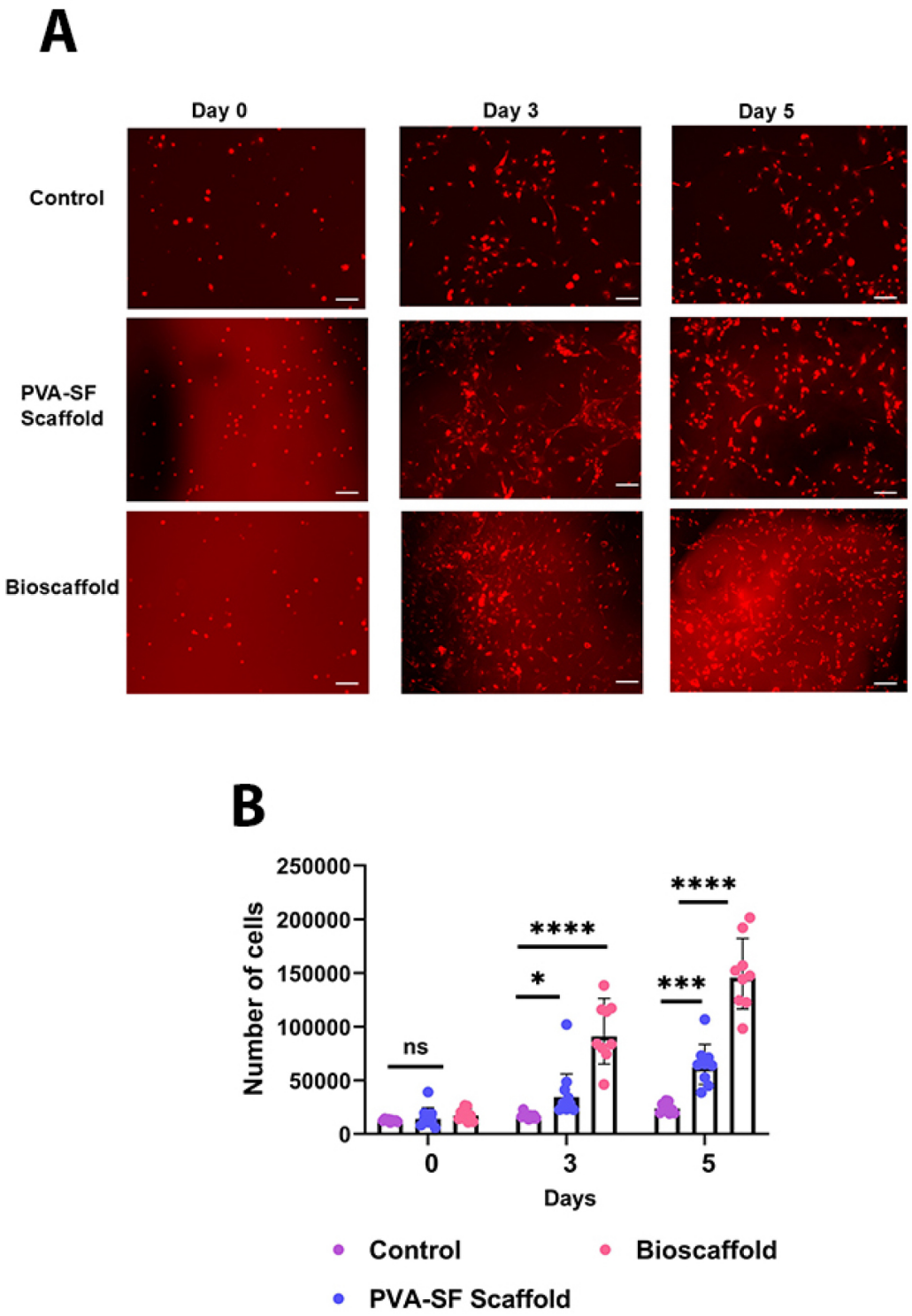

Fig. 10. Proliferation assay of the electrospun nanofibrous scaffolds. (A) Proliferation of DiI labelled AC-16 cells on nanofibrous scaffolds at different time points. Images captured at 4× magnification. Scale bar is 750 µm. (B) Quantitative scatter plot bar graphs showing AC-16 cells proliferation in different time points. Data presented as the number of cells in mean ± SD. Differences were compared using a two-way ANOVA, followed by Tukey's multiple comparisons test. Experiments were conducted in triplicate and repeated with three independent scaffolds. Control cells without any scaffold; Bioscaffold-combination of PVA-SF and natural compounds. ns - not significant, *$p < 0.05$, ***$p < 0.0001$ and ****$p < 0.00001$. DiI, 1,1′-Dioctadecyl-3,3,3′,3′-Tetramethylindocarbocyanine Perchlorate; AC-16, cardiomyocytes.

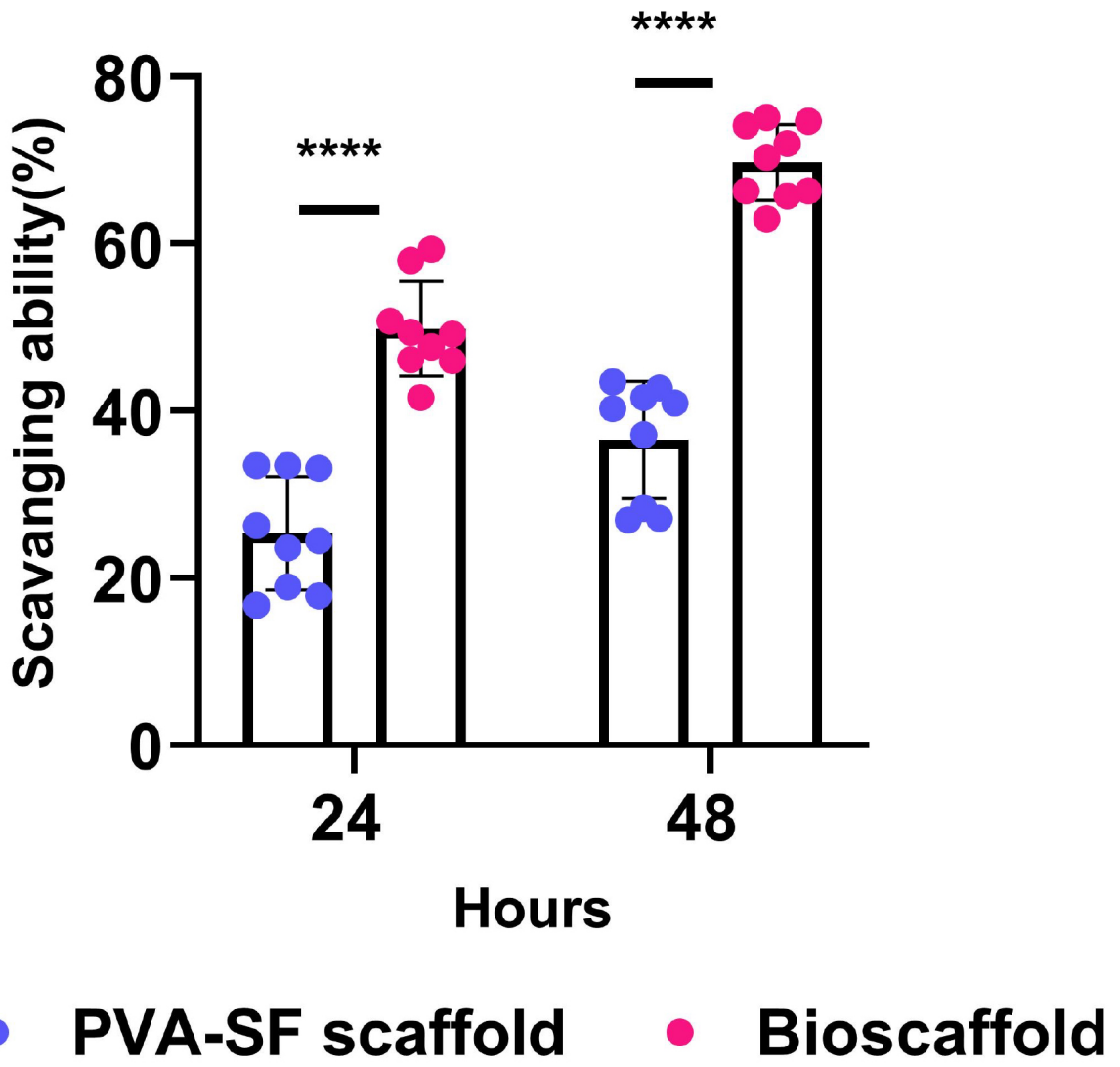

Fig. 11. Antioxidant activity analysis of the electrospun scaffolds. Quantitative scatter plot bar graphs showing the DPPH scavenging activity of scaffolds at 24 and 48 h. Comparison was done using a two-way ANOVA followed by uncorrected Fisher's LSD. Data are presented as a percentage of scavenging ability ± SD. Experiments were repeated in triplicate from three independent scaffolds. ****$p < 0.0001$. LSD, Least Significant Difference; DPPH, 1,1-diphenyl-2-picrylhydrazyl.

maintained its structural integrity, experiencing less than 30% degradation over 28 days, indicating its suitability for providing sustained therapeutic support during tissue healing. Thermal analyses (thermogravimetric analysis and differential scanning calorimetry) revealed that incorporating natural compounds, especially Manuka honey, increased the scaffold's glass transition temperature and thermal stability, potentially enhancing its flexibility and resistance to brittleness [45]. These properties are advantageous for clinical handling and applications requiring prolonged scaffold residence in the wound bed [60]. Functionally, the bioscaffold showed no cytotoxicity in HUVECs and human keratinocytes (HaCaT), fulfilling a fundamental requirement for biomedical use [50]. More importantly, it significantly enhanced endothelial cell migration at 24 hours and supported robust proliferation of human cardiomyocytes, aligning with its intended pro-regenerative role. The bioscaffold's antioxidant capacity was markedly higher than that of the control PVA-SF scaffold, suggesting it can mitigate ROS-mediated cellular damage, a key factor in chronic wound pathology [52]. Our findings support and extend prior studies that have incorporated individual natural compounds into electrospun scaffolds [57,61,62]. By combining these three agents with complementary mechanisms, we observed multifaceted functional benefits without compromising scaffold integrity or biocompatibility. This positions the developed bioscaffold as a promising platform for wound healing and potentially for targeted drug delivery, biosensors, and tissue engineering.

5. Limitations

The main limitation of our study is the lack of ghrelin-specific peak in the FTIR spectra, which was likely due to interference or overlap with the polymer spectra. However, the improvement in endothelial cell migration observed in a scratch assay suggests potential incorporation of Ghrelin, although these findings require further validation. Nevertheless, our functional assays demonstrated significant antioxidant and proangiogenic effects *in vitro*, indicating that the incorporated bioactive agents were released from the nanofiber scaffolds, remained biologically active, and were taken up by cells. Future investigation should focus on the controlled-release kinetics of the bioactive agents, on assessing the bioscaffold in *in vivo* wound-healing models, and on scaling up fabrication for clinical use.

6. Conclusions

In summary, we successfully fabricated a composite bioscaffold that integrates synthetic PVA with natural components, including silk fibroin, Manuka honey, and fenugreek seed extract with potential incorporation of Ghrelin. Although previous studies have incorporated individual natural compounds into electrospun scaffolds [57,61,62], to our knowledge, this is the first report of a bioscaffold with this combination as a mechanistic therapeutic strategy. A combination of these three agents, with complementary mechanisms, exhibited sustained degradation, enhanced angiogenesis, cell proliferation, and increased antioxidant capacity, without compromising scaffold integrity or biocompatibility, making it a strong candidate for wound healing and potentially for targeted drug delivery, biosensors, and tissue engineering.

Abbreviations

AC-16, Cardiomyocytes; ATR-FTIR, Attenuated total reflectance Fourier transform infrared spectroscopy; DiI, 1,1′-Dioctadecyl-3,3,3′,3′-Tetramethylindocarbocyanine Perchlorate; DMEM, Dulbecco's modified Eagle medium; DPPH, 1,1-diphenyl-2-picrylhydrazyl; DSC, Differential scanning calorimetry; ECM, Extracellular matrix; FBS, Fetal bovine serum; FTIR, Fourier-transform infrared; HaCaT, Human keratinocyte cell line; HUVEC, Human umbilical vein endothelial cell line; M200, Endothelial basal medium; MTT, 3-(4,5-dimethylthiazol-2-yl)-2,5-diphenyltetrazolium bromide; PBS, Phosphate buffer saline; PVA, Polyvinyl alcohol; ROS, Reactive oxygen species; SEM, Scanning electron microscopy; SF, Silk fibroin; T_g, The glass transition temperature; TGA, Thermogravimetric analysis.

Availability of Data and Materials

The datasets used and analyzed during the current study are available from the corresponding author on reasonable request.

Author Contributions

SS: Writing – original draft, Software, Formal analysis, Validation, Investigation, Methodology, Data curation. JAMS: Writing – original draft, Software, Formal analysis, Validation, Investigation, Methodology, Data curation. AA: Writing – review & editing, Conceptualisation, Resources, Supervision. RK: Writing – review & editing, Conceptualisation, Funding acquisition, Resources, Supervision. All authors read and approved the final manuscript. All authors have participated sufficiently in the work and agreed to be accountable for all aspects of the work.

Ethics Approval and Consent to Participate

Not applicable.

Acknowledgment

The authors would like to thank the Otago Electron Microscopy Team for their immense support with scanning electron microscopy and Manuka Med New Zealand for providing Manuka honey samples for this study. The graphic abstract was created with BioRender.com (Katare, R. (2026) https://BioRender.com/5s3toyf) and powerpoint.

Funding

This research was supported by funding from the Ministry of Business, Innovation and Employment NZ (UOOX2205). JAMS is supported by the PhD scholarship from the Heart Foundation NZ (Grant id-PJ-0000154).

Conflicts of Interest

All authors declare no conflicts of interest. Despite they received samples from Manuka Med New Zealand, the judgments in data interpretation and writing were not influenced by this relationship. Given his role as the Guest Editor and Editorial Board member, Rajesh Katare had no involvement in the peer-review of this article and has no access to information regarding its peer review. Full responsibility for the editorial process for this article was delegated to Francesca Diomede.

Declaration of AI and AI-Assisted Technologies in the Writing Process

During the preparation of this work, the authors used ChatGPT4.0 and Grammarly in order to check and correct the language and typographical and grammatical errors. After using this tool/service, the authors reviewed and edited the content as needed and take full responsibility for the content of the publication.

Supplementary Material

Supplementary material associated with this article can be found, in the online version, at https://doi.org/10.31083/FBL50459.

References

[1] Järbrink K, Ni G, Sönnergren H, Schmidtchen A, Pang C, Bajpai R, *et al*. Prevalence and incidence of chronic wounds and related complications: a protocol for a systematic review. Systematic Reviews. 2016; 5: 152. https://doi.org/10.1186/s13643-016-0329-y.

[2] Martinengo L, Olsson M, Bajpai R, Soljak M, Upton Z, Schmidtchen A, *et al*. Prevalence of chronic wounds in the general population: systematic review and meta-analysis of observational studies. Annals of Epidemiology. 2019; 29: 8–15. https://doi.org/10.1016/j.annepidem.2018.10.005.

[3] Jing Y, Lou Y, Chai X, Yunusov KE, Sun Y, Ruan L, *et al*. Stretchable and Self-Healing Conductive Composite Hydrogel Dressings Based on Cross-Linked Gelatin for Wound Closure Under Electrical Stimulation. Biomedical Materials & Devices. 2025; 3: 1422–1432. https://doi.org/10.1007/s44174-024-00265-2.

[4] Wang G, Yang F, Zhou W, Xiao N, Luo M, Tang Z. The initiation of oxidative stress and therapeutic strategies in wound healing. Biomedicine & Pharmacotherapy = Biomedecine & Pharmacotherapie. 2023; 157: 114004. https://doi.org/10.1016/j.biopha.2022.114004.

[5] Benichou G, Yamada Y, Yun SH, Lin C, Fray M, Tocco G. Immune recognition and rejection of allogeneic skin grafts. Immunotherapy. 2011; 3: 757–770. https://doi.org/10.2217/imt.11.2.

[6] Kapoor N, Yadav R. Manuka honey: A promising wound dressing material for the chronic nonhealing discharging wounds: A retrospective study. National Journal of Maxillofacial Surgery. 2021; 12: 233–237. https://doi.org/10.4103/njms.NJMS_154_20.

[7] Deng Y, Yang X, Zhang X, Cao H, Mao L, Yuan M, *et al*. Novel fenugreek gum-cellulose composite hydrogel with wound healing synergism: Facile preparation, characterization and wound healing activity evaluation. International Journal of Biological Macromolecules. 2020; 160: 1242–1251. https://doi.org/10.1016/j.ijbiomac.2020.05.220.

[8] Molan PC. The evidence supporting the use of honey as a wound dressing. The International Journal of Lower Extremity Wounds. 2006; 5: 40–54. https://doi.org/10.1177/1534734605286014.

[9] Majtan J. Honey: An immunomodulator in wound healing. Wound Repair and Regeneration. 2014; 22: 187–192. https://doi.org/10.1111/wrr.12117.

[10] Basch E, Ulbricht C, Kuo G, Szapary P, Smith M. Therapeutic applications of fenugreek. Alternative Medicine Review: a Journal of Clinical Therapeutic. 2003; 8: 20–27.

[11] Wani SA, Kumar P. Fenugreek: A review on its nutraceutical properties and utilization in various food products. Journal of the Saudi Society of Agricultural Sciences. 2018; 17: 97–106. https://doi.org/10.1016/j.jssas.2016.01.007.

[12] Neale JPH, Pearson JT, Thomas KN, Tsuchimochi H, Hosoda H, Kojima M, *et al*. Dysregulation of ghrelin in diabetes impairs the vascular reparative response to hindlimb ischemia in a mouse model; clinical relevance to peripheral artery disease. Scientific Reports. 2020; 10: 13651. https://doi.org/10.1038/s41598-020-70391-6.

[13] Liu C, Huang J, Li H, Yang Z, Zeng Y, Liu J, *et al*. Ghrelin accelerates wound healing through GHS-R1a-mediated MAPK-NF-κB/GR signaling pathways in combined radiation and burn injury in rats. Scientific Reports. 2016; 6: 27499. https://doi.org/10.1038/srep27499.

[14] Hematti P. Role of Extracellular Matrix in Cardiac Cellular Therapies. Advances in Experimental Medicine and Biology. 2018; 1098: 173–188. https://doi.org/10.1007/978-3-319-97421-7_9.

[15] Frangogiannis NG. The Extracellular Matrix in Ischemic and Nonischemic Heart Failure. Circulation Research. 2019; 125: 117–146. https://doi.org/10.1161/CIRCRESAHA.119.311148.

[16] Reddy MSB, Ponnamma D, Choudhary R, Sadasivuni KK. A Comparative Review of Natural and Synthetic Biopolymer Composite Scaffolds. Polymers. 2021; 13: 1105. https://doi.org/10.3390/polym13071105.

[17] Sun W, Gregory DA, Tomeh MA, Zhao X. Silk Fibroin as a Functional Biomaterial for Tissue Engineering. International Journal of Molecular Sciences. 2021; 22: 1499. https://doi.org/10.3390/ijms22031499.

[18] Jin SG. Production and Application of Biomaterials Based on Polyvinyl alcohol (PVA) as Wound Dressing. Chemistry, an Asian Journal. 2022; 17: e202200595. https://doi.org/10.1002/asia.202200595.

[19] Yunusov KE, Mirkholisov MM, Azizova MA, Jalilov JZ, Yarmatov SS, Todjiyev JN, *et al*. Advances in the formation and properties of nanofiber biomaterials from polyvinyl alcohol/carboxymethylcellulose/nanosilver systems for medical applications. Chemical Review and Letters. 2025; 8: 20–38. https://doi.org/10.22034/crl.2024.473962.1409.

[20] Sarymsakov AA, Yarmatov SS, Yunusov KE. Preparation and Physicochemical Properties of a Hemosorbent Derived from Bombyx mori Cocoon Fibroin. Russian Journal of Applied Chemistry. 2022; 95: 988–995. https://doi.org/10.1134/S1070427222070096.

[21] Sultan MT, Hong H, Lee OJ, Ajiteru O, Lee YJ, Lee JS, *et al*. Silk Fibroin-Based Biomaterials for Hemostatic Applications. Biomolecules. 2022; 12: 660. https://doi.org/10.3390/biom12050660.

[22] Sharma D, Srivastava S, Kumar S, Sharma PK, Hassani R, Dailah HG, *et al*. Biodegradable Electrospun Scaffolds as an Emerging Tool for Skin Wound Regeneration: A Comprehensive Review. Pharmaceuticals (Basel, Switzerland). 2023; 16: 325. https://doi.org/10.3390/ph16020325.

[23] Zainab I, Naseem Z, Batool SR, Waqas M, Nazir A, Nazeer MA. Polyurethane/silk fibroin-based electrospun membranes for wound healing and skin substitute applications. Beilstein Journal of Nanotechnology. 2025; 16: 591–612. https://doi.org/10.3762/bjnano.16.46.

[24] Yang X, Fan L, Ma L, Wang Y, Lin S, Yu F, *et al*. Green electrospun Manuka honey/silk fibroin fibrous matrices as potential wound dressing. Materials & Design. 2017; 119: 76–84. https://doi.org/10.1016/j.matdes.2017.01.023.

[25] Selvaraj S, Fathima NN. Fenugreek Incorporated Silk Fibroin Nanofibers-A Potential Antioxidant Scaffold for Enhanced Wound Healing. ACS Applied Materials & Interfaces. 2017; 9: 5916–5926. https://doi.org/10.1021/acsami.6b16306.

[26] Islam MT, Sharmin AA, Laing R, McConnell M, Ali MA. Bead-Free Electrospun Nanofibrous Scaffold Made of PVOH/Keratin/Chitosan Using a Box–Behnken Experimental Design and In Vitro Studies. Polysaccharides. 2024; 5: 112–128. https://doi.org/10.3390/polysaccharides5020009.

[27] Zhang KH, Yu QZ, Mo XM. Fabrication and intermolecular interactions of silk fibroin/hydroxybutyl chitosan blended nanofibers. International Journal of Molecular Sciences. 2011; 12: 2187–2199. https://doi.org/10.3390/ijms12042187.

[28] Chatterley AS, Laity P, Holland C, Weidner T, Woutersen S, Giubertoni G. Broadband Multidimensional Spectroscopy Identifies the Amide II Vibrations in Silkworm Films. Molecules (Basel, Switzerland). 2022; 27: 6275. https://doi.org/10.3390/molecules27196275.

[29] Komissarova EV, Saha SK, Rossman TG. Dead or dying: the importance of time in cytotoxicity assays using arsenite as an example. Toxicology and Applied Pharmacology. 2005; 202: 99–107. https://doi.org/10.1016/j.taap.2004.06.010.

[30] Davidson MM, Nesti C, Palenzuela L, Walker WF, Hernandez

E, Protas L, *et al*. Novel cell lines derived from adult human ventricular cardiomyocytes. Journal of Molecular and Cellular Cardiology. 2005; 39: 133–147. https://doi.org/10.1016/j.yjmcc.2005.03.003.

[31] Kastury N, Hidalgo V, Pandi B, Li L, Lam MPY, Lau E. Senescence in human AC16 cardiac cells is associated with thymidine kinase induction and histone loss. MicroPublication Biology. 2023; 2023: 10.17912/micropub.biology.000865. https://doi.org/10.17912/micropub.biology.000865.

[32] Noriega SE, Hasanova GI, Schneider MJ, Larsen GF, Subramanian A. Effect of fiber diameter on the spreading, proliferation and differentiation of chondrocytes on electrospun chitosan matrices. Cells, Tissues, Organs. 2012; 195: 207–221. https://doi.org/10.1159/000325144.

[33] Guo Z, Ma M, Huang X, Li H, Zhou C. Effect of Fiber Diameter on Proliferation and Differentiation of MC3T3-E1 Pre-Osteoblasts. Journal of Biomaterials and Tissue Engineering. 2017; 7: 162–169. https://doi.org/10.1166/jbt.2017.1548.

[34] Ameer JM, Pr AK, Kasoju N. Strategies to Tune Electrospun Scaffold Porosity for Effective Cell Response in Tissue Engineering. Journal of Functional Biomaterials. 2019; 10: 30. https://doi.org/10.3390/jfb10030030.

[35] El-Bahy GMS. FTIR and Raman spectroscopic study of Fenugreek (Trigonella foenum graecum L.) seeds. Journal of Applied Spectroscopy. 2005; 72: 111–116. https://doi.org/10.1007/s10812-005-0040-6.

[36] Ghalei S, Li J, Douglass M, Garren M, Handa H. Synergistic Approach to Develop Antibacterial Electrospun Scaffolds Using Honey and *S*-Nitroso-*N*-acetyl Penicillamine. ACS Biomaterials Science & Engineering. 2021; 7: 517–526. https://doi.org/10.1021/acsbiomaterials.0c01411.

[37] Sayed MM, Mousa HM, El-Aassar MR, El-Deeb NM, Ghazaly NM, Dewidar MM, *et al*. Enhancing mechanical and biodegradation properties of polyvinyl alcohol/silk fibroin nanofibers composite patches for Cardiac Tissue Engineering. Materials Letters. 2019; 255: 126510. https://doi.org/10.1016/j.matlet.2019.126510.

[38] Kale RD, Gorade VG, Parmaj O. Development and characterization study of silk filament reinforced chitosan biocomposite. Journal of Natural Fibers. 2020; 17: 66–74. https://doi.org/10.1080/15440478.2018.1465878.

[39] Vadivel D, Djemal R, García J, Pagano A, Trabelsi R, Gdoura-Ben Amor M, *et al*. Exploring seed characteristics and performance through advanced physico-chemical techniques. Scientific Reports. 2024; 14: 24162. https://doi.org/10.1038/s41598-024-75236-0.

[40] Tomczyk M, Czerniecka-Kubicka A, Miłek M, Sidor E, Dżugan M. Tracking of Thermal, Physicochemical, and Biological Parameters of a Long-Term Stored Honey Artificially Adulterated with Sugar Syrups. Molecules (Basel, Switzerland). 2023; 28: 1736. https://doi.org/10.3390/molecules28041736.

[41] Tomaszewska-Gras J, Bakier S, Goderska K, Mansfeld K. Differential Scanning Calorimetry for Determining the Thermodynamic Properties of Selected Honeys. Journal of Apicultural Science. 2015; 59: 109–118. https://doi.org/10.1515/jas-2015-0012.

[42] Xu X, Sun Q, Xu A, Guo X. Biodegradable and Biocompatible Polyvinyl alcohol/ Silk Fibroin-Based Composite with Improved Strength. Journal of Polymer Materials. 2022; 39: 167–181. https://doi.org/10.32381/JPM.2022.39.1-2.11.

[43] Kandile NG, Nasr AS. Poly(vinyl alcohol) membranes-inspired heterocyclic compounds for different applications: synthesis and characterization. Polymer Bulletin. 2023; 80: 2367–2387. https://doi.org/10.1007/s00289-022-04143-z.

[44] Irantash S, Gholipour-Kanani A, Najmoddin N, Varsei M. A hybrid structure based on silk fibroin/PVA nanofibers and alginate/gum tragacanth hydrogel embedded with cardamom extract. Scientific Reports. 2024; 14: 14010. https://doi.org/10.1038/s41598-024-63061-4.

[45] Sarhan WA, Azzazy HME, El-Sherbiny IM. The effect of increasing honey concentration on the properties of the honey/polyvinyl alcohol/chitosan nanofibers. Materials Science & Engineering. C, Materials for Biological Applications. 2016; 67: 276–284. https://doi.org/10.1016/j.msec.2016.05.006.

[46] Ghanghas N, Prabhakar PK, Sharma S, Mukilan MT. Microfluidization of fenugreek (Trigonella foenum graecum) seed protein concentrate: Effects on functional, rheological, thermal and microstructural properties. LWT. 2021; 149: 111830. https://doi.org/10.1016/j.lwt.2021.111830.

[47] Gyeong-Man K. Fabrication of Bio-Nanocomposite Nanofibers Mimicking the Mineralized Hard Tissues via Electrospinning Process. In Ashok K (ed.) Nanofibers (pp. Ch. 4). IntechOpen: Rijeka. 2010.

[48] Gupta B, Agarwal R, Sarwar Alam M. Preparation and characterization of polyvinyl alcohol-polyethylene oxide-carboxymethyl cellulose blend membranes. Journal of Applied Polymer Science. 2013; 127: 1301–1308. https://doi.org/10.1002/app.37665.

[49] Remiš T, Bělský P, Kovářík T, Kadlec J, Ghafouri Azar M, Medlín R, *et al*. Study on Structure, Thermal Behavior and Viscoelastic Properties of Nanodiamond-Reinforced Poly (vinyl alcohol) Nanocomposites. Polymers. 2021; 13: 1426. https://doi.org/10.3390/polym13091426.

[50] Litowczenko J, Woźniak-Budych MJ, Staszak K, Wieszczycka K, Jurga S, Tylkowski B. Milestones and current achievements in development of multifunctional bioscaffolds for medical application. Bioactive Materials. 2021; 6: 2412–2438. https://doi.org/10.1016/j.bioactmat.2021.01.007.

[51] Diller RB, Tabor AJ. The Role of the Extracellular Matrix (ECM) in Wound Healing: A Review. Biomimetics (Basel, Switzerland). 2022; 7: 87. https://doi.org/10.3390/biomimetics7030087.

[52] Hunt M, Torres M, Bachar-Wikstrom E, Wikstrom JD. Cellular and molecular roles of reactive oxygen species in wound healing. Communications Biology. 2024; 7: 1534. https://doi.org/10.1038/s42003-024-07219-w.

[53] Schilrreff P, Alexiev U. Chronic Inflammation in Non-Healing Skin Wounds and Promising Natural Bioactive Compounds Treatment. International Journal of Molecular Sciences. 2022; 23: 4928. https://doi.org/10.3390/ijms23094928.

[54] Lee PC, Salyapongse AN, Bragdon GA, Shears LL, 2nd, Watkins SC, Edington HD, *et al*. Impaired wound healing and angiogenesis in eNOS-deficient mice. The American Journal of Physiology. 1999; 277: H1600–H1608. https://doi.org/10.1152/ajpheart.1999.277.4.H1600.

[55] Parvinzadeh Gashti M, Dehdast SA, Berenjian A, Shabani M, Zarinabadi E, Chiari Fard G. PDDA/Honey Antibacterial Nanofiber Composites for Diabetic Wound-Healing: Preparation, Characterization, and In Vivo Studies. Gels. 2023; 9: 173. https://doi.org/10.3390/gels9030173.

[56] Lan D, Zhang Y, Zhang H, Zhou J, Chen X, Li Z, *et al*. Silk fibroin/polycaprolactone nanofibrous membranes loaded with natural Manuka honey for potential wound healing. Journal of Applied Polymer Science. 2022; 139: 51686. https://doi.org/10.1002/app.51686.

[57] Kassem LM, El-Deen AG, Zaki AH, El-Dek SI. Electrospun manuka honey@PVP nanofibers enclosing chitosan-titanate for highly effective wound healing. Cellulose. 2023; 30: 6487–6505. https://doi.org/10.1007/s10570-023-05267-9.

[58] Zhang Y, Chen Y, Li K, Chen C, Hu Y, Li X. Ghrelin promotes chronic diabetic wound healing by regulating keratinocyte proliferation and migration through the ERK1/2 pathway. Pep-

tides. 2025; 184: 171350. https://doi.org/10.1016/j.peptides.2025.171350.

[59] Kiang JG, Smith JT, Cannon G, Anderson MN, Ho C, Zhai M, *et al*. Ghrelin, a novel therapy, corrects cytokine and NF-κB-AKT-MAPK network and mitigates intestinal injury induced by combined radiation and skin-wound trauma. Cell & Bioscience. 2020; 10: 63. https://doi.org/10.1186/s13578-020-00425-z.

[60] Negut I, Dorcioman G, Grumezescu V. Scaffolds for Wound Healing Applications. Polymers. 2020; 12: 2010. https://doi.org/10.3390/polym12092010.

[61] Minden-Birkenmaier BA, Smith RA, Radic MZ, van der Merwe M, Bowlin GL. Manuka Honey Reduces NETosis on an Electrospun Template Within a Therapeutic Window. Polymers. 2020; 12: 1430. https://doi.org/10.3390/polym12061430.

[62] Parangusan H, Karuppasamy K, Bhadra J. Fenugreek-enriched electrospun PLA scaffold: revolutionizing tissue engineering solutions. Journal of Polymer Research. 2025; 32: 175. https://doi.org/10.1007/s10965-025-04373-5.